
TROI: CROSS-SUBJECT PRETRAINING WITH SPARSE VOXEL SELECTION FOR ENHANCED fMRI VISUAL DECODING

Ziyu Wang, Tengyu Pan, Zhenyu Li, Jianyong Wang¹, Xiuxing Li², and Ji Wu³

¹ Department of Computer Science and Technology, Tsinghua University, Beijing, China

² School of Computer Science and Technology, Beijing Institute of Technology, Beijing, China

³ School of Computer Science and Engineering, Beihang University, Beijing, China

ABSTRACT

fMRI (functional Magnetic Resonance Imaging) visual decoding involves decoding the original image from brain signals elicited by visual stimuli. This often relies on manually labeled ROIs (Regions of Interest) to select brain voxels. However, these ROIs can contain redundant information and noise, reducing decoding performance. Additionally, the lack of automated ROI labeling methods hinders the practical application of fMRI visual decoding technology, especially for new subjects. This work presents TROI (Trainable Region of Interest), a novel two-stage, data-driven ROI labeling method for cross-subject fMRI decoding tasks, particularly when subject samples are limited. TROI leverages labeled ROIs in the dataset to pretrain an image decoding backbone on a cross-subject dataset, enabling efficient optimization of the input layer for new subjects without retraining the entire model from scratch. In the first stage, we introduce a voxel selection method that combines sparse mask training and low-pass filtering to quickly generate the voxel mask and determine input layer dimensions. In the second stage, we apply a learning rate rewinding strategy to fine-tune the input layer for downstream tasks. Experimental results on the same small sample dataset as the baseline method for brain visual retrieval and reconstruction tasks show that our voxel selection method surpasses the state-of-the-art method MindEye2 with an annotated ROI mask.

Keywords First keyword · Second keyword · More

1 Introduction

Decoding visual stimuli from measured brain activity has long been a central focus in computational neuroscience. Recently, significant progress has been made in decoding techniques that focus on functional magnetic resonance imaging (fMRI) data. fMRI is a type of neuroimaging that reflects neural activity by measuring changes in brain oxygenation levels [1]. Recent methods [2, 3, 4, 5, 6] attempt to establish a mapping relationship between fMRI brain activity patterns and the latent space of pretrained deep learning models, for the purpose of retrieving and reconstructing visual stimuli corresponding to brain activity, as Fig. 1 shows.

While these methods have demonstrated notable success, they encounter limitations when applied to new subjects due to individual variations in brain shape and functional organization. To mitigate this issue, existing approaches often rely on regions of interest (ROIs) to perform decoding, which helps reduce the impact of structural and functional differences across subjects. Common techniques include anatomical template-based ROI analysis [7, 8], functional-based ROI analysis [9, 10, 11], and data-driven ROI analysis [12, 13]. However, these methods either neglect subject-specific variations or focus exclusively on regions associated with simple visual stimuli. For more complex decoding tasks, such as image reconstruction, the selected ROIs may contain redundant and noisy voxels, and the large encoding space of task events can lead to suboptimal performance.

To address these issues, we propose a two-stage data-driven ROI labeling method called Trainable Region of Interest (TROI). This method is for cross-subject fMRI decoding tasks, even with limited samples from a new subject. Before labeling for the new subject, we pretrain an fMRI decoding backbone on a cross-subject dataset to focus on



Figure 1: Visual reconstructions from fMRI using baseline MindEye2 w/w/o our proposed TROI in different training data volume.

optimizing the brain voxel mask rather than training the entire model from scratch. In the first stage, we apply LASSO regularization[14] for sparse mask training and use a low-pass filter to quickly obtain the voxel mask and determine the input layer dimensions. In the second stage, we fine-tune the input layer for downstream tasks using a learning rate rewinding strategy. When evaluated on small samples from the NSD dataset using the state-of-the-art fMRI decoding model, MindEye2, our approach outperforms methods with annotated ROIs in both retrieval and reconstruction tasks.

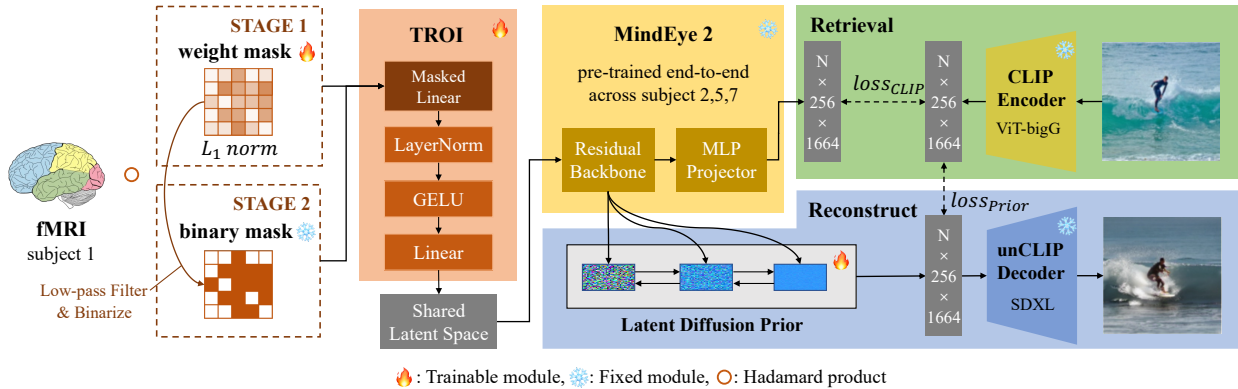


Figure 2: Overview of TROI module structure followed by a residual MLP backbone and two task-specific submodules. Taking Subject 1 as a new subject, the cross-subject backbone network is trained using data from Subjects 2, 3, 5, and 7. The subject-specific TROI module is then trained in two stages with small sample data from Subject 1.

2 Approach

As shown in Fig. 2, our model maps brain activity into an embedding space using the subject-specific TROI and subject-shared residual Multiple Layer Perceptron (MLP) backbone networks. It then integrates various downstream tasks, such as retrieval and reconstruction, to facilitate cross-modal learning with image-based supervision signals. We begin by pretraining the backbone using data from multiple subjects, excluding one subject as a reserved subject. Then, we fine-tune the model using a subset of data from the reserved subject to simulate handling limited data from a new subject.

2.1 Cross-subject pretraining

Denote the baseline network as \mathcal{B} , a pretrained CLIP image encoder as \mathcal{C} . Suppose we have n subjects, and the dataset from i -th subject are $\mathcal{D}_i = \{x_{i,j}, y_{i,j}\}$, where j refers to the j -th data point, $x_{i,j}$ and $y_{i,j}$ refer to fMRI and image sample of i -th subject and j -th data point respectively. We flatten the spatial patterns of $x_{i,j}$ and then align them to a shared latent space through subject-specific networks named as $TROI_i$ with the parameters w_i , to address the varying fMRI size of different subjects. We use MixCo[15], a linear interpolation method, to augment the data. For subject i , suppose the sample size is s_i . We mix the fMRI data $x_{i,j}$ of the same subject i but different data point j , as shown in Eq. (1).

$$x_{i,j}^* = \lambda_{i,j}x_{i,j} + (1 - \lambda_{i,j})x_{i,k_j}, \lambda \sim Beta(\alpha, \beta). \quad (1)$$

Here k_j is an arbitrary mixing index for the j -th data, and $\lambda_{i,j}$ represents the j -th mixing weight, which is sampled from a Beta distribution with hyperparameter $\alpha = \beta = 0.2$. The embedding of fMRI and image is calculated as $b_{i,j}^* = \mathcal{B}(TROI_i(x_{i,j}^*))$ and $c_{i,j} = \mathcal{C}(y_{i,j})$ respectively.

To address the challenge of learning an embedding space that can satisfy the objectives of both tasks [2], we incorporate an MLP Projector module \mathcal{H} to decouple the feature spaces for retrieval and reconstruction. The projected embedding of fMRI is calculated as $h_{i,j}^* = \mathcal{H}(b_{i,j}^*)$.

2.1.1 Retrieval

In the retrieval task, our goal is to retrieve the corresponding image from a set of images based on a given fMRI data, and vice versa. To achieve this, we use the CLIP loss with MixCo to maximize the cosine similarity between matching pairs and minimize it for non-matching pairs, as shown in Eq. (2).

$$\mathcal{L}_{CLIP} = \mathcal{L}_{MixCo}(h_{i,j}^*, c_{i,j}) \quad (2)$$

Here, \mathcal{L}_{MixCo} is the loss function introduced in study [15], $h_{i,j}^*$ and $c_{i,j}$ are l2-normalized and τ is a temperature hyperparameter. The study in [16] mentions that mix-up augment can negatively impact the performance of generative tasks. To balance the performance of the two downstream tasks, we stop using the mix-up data augmentation method after one-third of the training process.

2.1.2 Reconstruction

In the reconstruction task, our goal is to reconstruct the image corresponding to what the subject saw based on the given fMRI data. Following DALL-E 2 [17], we use a diffusion prior to map the fMRI embedding space to the image embedding space. Afterward, we use an unCLIP decoder to reconstruct the images.

To maintain the consistency between the reconstructed image and the original image, we minimize the Euclidean distance between the fMRI embedding vector and the corresponding image embedding. Denote latent diffusion prior network as \mathcal{P} with the parameters Ω , the loss of reconstruction is calculated as follows.

$$\mathcal{L}_{Prior} = \sum_{i=1}^n \sum_{j=1}^{s_i} (\mathcal{P}(b_{i,j}^*) - (\lambda c_{i,j} + (1 - \lambda)c_{i,k_j}))^2, \quad (3)$$

Here, k_j is an arbitrary mixing index for the j -th data, consistent with the definition in Eq. (1).

During training, we optimize the model parameters \mathcal{M}, w, Ω jointly by minimizing the losses from both tasks, balanced by a hyperparameter ε , as shown in Eq. (4).

$$\mathcal{L}(\mathcal{M}, w, \Omega; \mathcal{B}, \mathcal{H}, \mathcal{C}, \mathcal{D}) = \mathcal{L}_{CLIP} + \varepsilon \mathcal{L}_{Prior}, \quad (4)$$

2.2 Stage1: Sparse Mask Training

Utilizing all brain voxels as input for model training introduces considerable noise, which can lead to overfitting, particularly in scenarios with limited sample sizes. To mitigate this issue, we employ a 0-1 ROI mask \mathcal{M}' to selectively extract voxels from coarsely segmented brain regions, with a primary focus on the occipital lobe [18]. This mask is applied to the input data through an element-wise multiplication (Hadamard product), resulting in a new input representation $\hat{x}_i = x_i \circ \mathcal{M}'$.

When given a voxel number budget V , the problem of determining the number of filters can be formulated as a mixed 0-1 binary optimization problem. The objective is to select a set of voxels that minimizes the decoding task loss function, while ensuring that the number of voxels in the mask does not exceed V , as shown in Eq. (5).

$$\begin{aligned} \min_{\mathcal{M}', w, \Omega} \quad & \mathcal{L}(\mathcal{M}', w, \Omega; \mathcal{B}, \mathcal{H}, \mathcal{C}, \mathcal{D}), \\ \text{s.t.} \quad & \|\mathcal{M}'\|_0 \leq V, \end{aligned} \quad (5)$$

However, since the loss function in Eq. (5) cannot be directly optimized via gradient-based methods, we introduce a weighted ROI mask, denoted as \mathcal{M} . The loss function for the optimization problem is formulated by introducing an LASSO coefficient, denoted as ψ , to adjust the optimization process.

$$\mathcal{L}_{total} = \mathcal{L}(\mathcal{M}, w, \Omega; \mathcal{B}, \mathcal{H}, \mathcal{C}, \mathcal{D}) + \psi \|\mathcal{M}\|_1, \quad (6)$$

To accelerate the sparsification of \mathcal{M} , in each iteration, we set the elements of \mathcal{M} that are less than a fixed threshold th to zero. \mathcal{M}' can be calculated from \mathcal{M} , as shown in Eq. (7).

$$\mathcal{M}'[i] = \begin{cases} 1 & \text{if } \mathcal{M}[i] > th \\ 0 & \text{otherwise} \end{cases} \quad (7)$$

In scenarios with limited training data, the weighted mask \mathcal{M} may learn incorrect weights due to overfitting. In such cases, directly applying a fixed threshold for binarization can result in a voxel mask \mathcal{M}' that includes incorrect voxels, leading to poor performance. To address this issue, we apply a low-pass filter G to \mathcal{M} before binarization. This step leverages the spatial locality of brain functional regions, incorporating prior information from the data to mitigate overfitting. The proposed algorithm proceeds iteratively, as shown in Algorithm 1.

Algorithm 1 Sparse Mask Training

Require: Pretrained backbone \mathcal{B} and projector \mathcal{H} , Pretrained CLIP image encoder \mathcal{C} , Small sample training dataset \mathcal{D}

- 1: initialize \mathcal{M} and \mathcal{M}' as all ones
- 2: **while** $\|\mathcal{M}'\|_0 > V$ **do**
- 3: $\mathcal{M}^*, w^*, \Omega^* \leftarrow \arg \min \mathcal{L}_{total}(\mathcal{M}, w, \Omega; \mathcal{B}, \mathcal{H}, \mathcal{C}, \mathcal{D})$ {Optimize with Eq. (6)}
- 4: $\mathcal{M}^*[i] = \begin{cases} \mathcal{M}^*[i] & \text{if } \mathcal{M}^*[i] > th \\ 0 & \text{otherwise} \end{cases}$
- 5: $\mathcal{M}, w, \Omega \leftarrow \mathcal{M}^*, w^*, \Omega^*$
- 6: $\mathcal{M}' \leftarrow \mathcal{M} * G$ {Use Gaussian kernel G as low-pass filter}
- 7: $\mathcal{M}'[i] = \begin{cases} 1 & \text{if } \mathcal{M}'[i] > th \\ 0 & \text{otherwise} \end{cases}$
- 8: **end while**

Ensure: Brain voxel mask \mathcal{M}'

Our approach is similar to the sparse mask training techniques commonly used in model pruning[19, 20]. However, instead of applying sparsity constraints to the weights of linear layers, we directly impose a sparse mask on the input data. This allows us to leverage the spatial locality of brain activity to further denoise the learned mask.

2.3 Stage2-Learning Rate Rewinding

A recent study [21] suggests that retraining a model with a sparse mask from scratch outperforms fine-tuning approaches. This retraining strategy, known as learning rate rewinding, leads to improved model performance. Building on this, we retrain the TROI module from scratch using the mask \mathcal{M}' trained in Stage 1, which reduces the number of voxels in the fMRI input during Stage 2.

3 Experiments

3.1 Experiments Setting

We conducted the training on a single machine equipped with an L40 GPU (48GB). Taking Subject 1 as the target subject in our experiment as an example, for the cross-subject pretraining process, we trained the model for 150 epochs using the training data from Subjects 2, 5, and 7, with annotated ROIs in the dataset serving as voxel selectors. The same procedure applies when using other subjects as the target. We then used Subject 1 as a new subject for small sample learning. In Stage 1, with a batch size of 24, we reduced the number of voxels in the mask to approximately 3,000 in about 15 epochs. In Stage 2, we continued training for 150 epochs with a batch size of 24 before stopping.

3.2 Dataset

We use the Natural Scenes Dataset (NSD) [11], which comprises 30,000 fMRI scans across 40 sessions from 8 subjects. Each image is viewed three times during data collection, with the viewings spaced apart. All images in the dataset

Table 1: Evaluation result on dataset from subjects 1,2,5 and 7. A bolded number indicates a better result. (↑) indicates that a higher value is preferable, and (↓) indicates that a lower value is better.

metrics	retrieval		reconstruction			
	image ↑	brain ↑	PixCorr ↑	SSIM ↑	Incep ↑	SwAV ↓
subj1	94.0%	77.6%	0.235	0.428	83.6%	0.459
w TROI	93.6%	85.3%	0.206	0.382	85.9%	0.431
subj2	90.5%	67.2%	0.200	0.433	81.9%	0.467
w TROI	91.3%	74.3%	0.171	0.387	82.2%	0.461
subj5	66.9%	47.0%	0.175	0.405	84.3%	0.444
w TROI	67.3%	47.7%	0.161	0.376	84.5%	0.454
subj7	64.4%	37.8%	0.170	0.408	74.9%	0.504
w TROI	67.3%	51.7%	0.168	0.373	80.1%	0.471

Table 2: Quantitative comparison regarding the pretrained backbone (PT), low-pass filtering (LPF), and learning rate rewinding (LRR) techniques. Results are based on the first 1-hour data of Subject 1, with the ROI mask containing 3,000 voxels.

metrics	retrieval		reconstruction			
	image ↑	brain ↑	PixCorr ↑	SSIM ↑	Incep ↑	SwAV ↓
Ours	93.6%	85.3%	0.206	0.382	85.9%	0.431
w/o PT	81.7%	70.7%	0.176	0.431	74.9%	0.467
w/o LPF	89.3%	78.7%	0.174	0.321	83.6%	0.441
+ w/o LRR	63.3%	44.3%	0.130	0.298	75.1%	0.504

are sourced from the Microsoft COCO dataset [22]. The fMRI data have a resolution of 1.8mm, and we perform voxel-wise z-score normalization and a rough segmentation of the brain (primarily the occipital lobe), resulting in data with dimensions of 60×40×40. This preprocessing step requires only a manual check of individual fMRI scans and does not demand precise expertise or significant manual labor. The ROI collections provided in the NSD dataset were manually defined on fsaverage, with functional divisions based on anatomical structures. These include a set of ROIs corresponding to major sulci and gyri, as well as streams, a collection of ROIs reflecting large-scale divisions of the visual cortex (such as early, midventral, midlateral, etc.). Our cross-subject backbone pretraining process and baseline MindEye2 are both based on these ROI annotations.

3.3 Result

3.3.1 Evaluation Metrics

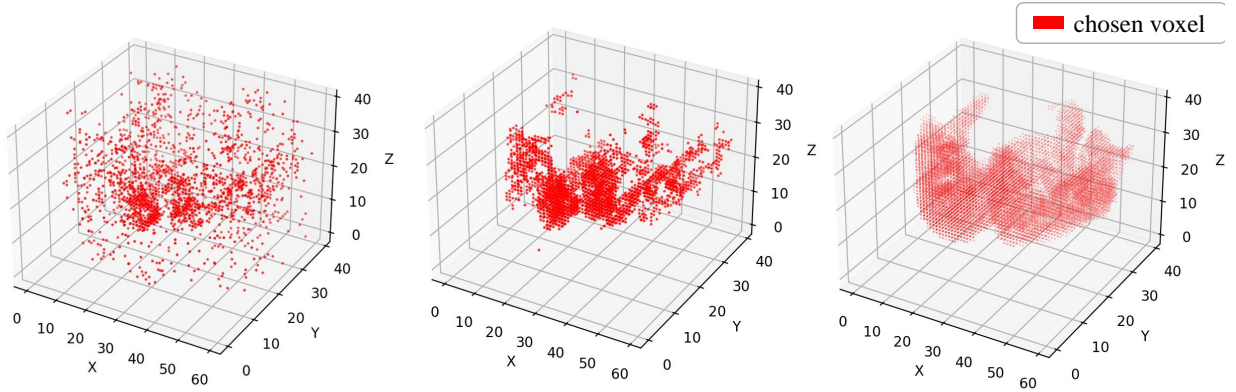
We follow the same evaluation metrics as recent works [2, 3, 4, 5, 6], as shown in Table 2. In the retrieval task, **image retrieval** refers to the percentage of correct image retrievals out of 300 candidates given the associated brain sample (chance = 0.3%), vice-versa for **brain retrieval**. In the reconstruction task, **PixCorr** represents the pixel-wise correlation between the ground truth and reconstructions, and **SSIM** refers to the Structural Similarity Index Metric [23]. **SwAV** represents the average correlation distance of features derived from SwAV-ResNet50’s[24] feature space, while **Incep** refers to two-way identification (chance = 50%) using Inception V3 [25].

3.3.2 Comparison with baselines

Fig. 1 shows that we can accurately reconstruct visual stimuli, and we slightly outperform MindEye2 in small sample scenarios. Table 1 shows how our method performs on different subject. Each experiment involves pretraining the backbone on datasets excluding the target subject, followed by fine-tuning the TROI using the first 1-hour data from the target subject’s dataset, and finally evaluating on the full dataset of the target subject.

3.3.3 Visualization of trained ROI

Fig. 3 reveals that the filtered mask we trained shows a higher consistency with the annotated ROI masks in terms of spatial location compared to the unfiltered mask, which highlights the necessity of applying low-pass filtering to refine the mask, as it helps eliminate noise. The significant reduction in voxel count demonstrates our method’s ability to effectively select vision-related voxels from coarsely segmented brain region aligning with findings from prior neuroscience studies[18].



voxel num=3000 (not filtered) voxel num=3000 (filtered) voxel num=15732 (origin)

Figure 3: TROI mask trained with the first 1h data of subject 1

Table 3: Quantitative comparison *w.r.t* different ROI mask. Results were derived from the first 1h data of Subject 1.

metrics		voxel number budget			
		1000	2000	3000	baseline
retrieval	image \uparrow	90.3%	93.7%	93.6%	94.0%
	brain \uparrow	76.5%	84.7%	85.3%	77.6%
recon	PixCorr \uparrow	0.198	0.213	0.206	0.235
	SSIM \uparrow	0.376	0.388	0.382	0.428
	Incep \uparrow	78.7%	83.8%	85.9%	83.6%
	SwAV \downarrow	0.504	0.477	0.431	0.459

3.4 Ablation Study

Impact of pretrained backbone, low-pass filtering and learning rate rewinding Table 2 shows that utilizing the pretrained backbone network improves the model’s performance across all metrics in the small-sample scenario, confirming the effectiveness of our pretraining approach. Table 2 also shows that low-pass filter and learning rate rewinding method contribute to improving the model’s decoding performance from fMRI data. Although the learning rate rewinding approach incurs additional training costs, our experimental results demonstrate that it is essential for effective decoding in small-sample scenarios.

Impact of voxel number budget Table 3 shows that the decoding performance improves consistently with an increasing voxel number budget. Interestingly, the model utilizing only 3,000 voxels already outperforms the baseline model that relies on the original ROI. These results support our hypothesis that a substantial fraction of voxels within the annotated ROI contribute minimally to the decoding task.

4 Conclusion

This paper introduces a data-driven ROI labeling approach, termed TROI, designed to decode fMRI brain visual activity in new subjects, especially when ROI annotations are unavailable and the training data is limited. To mitigate noise, we applied the sparse mask training and learning rate rewinding method, significantly reducing the number of brain voxels in the input data. Additionally, by employing a cross-subject pretraining method, we minimized the model’s trainable parameters in small-sample fine-tuning, effectively mitigating the risk of over-fitting. Using MindEye2, the state-of-the-art model for fMRI visual decoding, as our baseline, we trained on a small sample dataset from NSD and surpass the annotated ROI’s performance, particularly in terms of brain retrieval metrics.

Acknowledgment

This work was supported in part by National Key Research and Development Program of China under Grant No. 2020YFA0804503, National Natural Science Foundation of China under Grant No. 62272264, and Beijing Academy of Artificial Intelligence (BAAI).

References

- [1] Shuo Huang, Wei Shao, Mei-Ling Wang, and Dao-Qiang Zhang. fmri-based decoding of visual information from human brain activity: A brief review. *International Journal of Automation and Computing*, 18(2):170–184, 2021.
- [2] Paul Scotti, Atmadeep Banerjee, Jimmie Goode, Stepan Shabalin, Alex Nguyen, Aidan Dempster, Nathalie Verlinde, Elad Yundler, David Weisberg, Kenneth Norman, et al. Reconstructing the mind’s eye: fmri-to-image with contrastive learning and diffusion priors. *Advances in Neural Information Processing Systems*, 36, 2024.
- [3] Paul S Scotti, Mihir Tripathy, Cesar Kadir Torrico Villanueva, Reese Kneeland, Tong Chen, Ashutosh Narang, Charan Santhirasegaran, Jonathan Xu, Thomas Naselaris, Kenneth A Norman, et al. Mindeye2: Shared-subject models enable fmri-to-image with 1 hour of data. *arXiv preprint arXiv:2403.11207*, 2024.
- [4] Furkan Ozcelik, Bhavin Choksi, Milad Mozafari, Leila Reddy, and Rufin VanRullen. Reconstruction of perceived images from fmri patterns and semantic brain exploration using instance-conditioned gans. In *2022 International Joint Conference on Neural Networks (IJCNN)*, pages 1–8. IEEE, 2022.
- [5] Furkan Ozcelik and Rufin VanRullen. Natural scene reconstruction from fmri signals using generative latent diffusion. *Scientific Reports*, 13(1):15666, 2023.
- [6] Reese Kneeland, Jordyn Ojeda, Ghislain St-Yves, and Thomas Naselaris. Reconstructing seen images from human brain activity via guided stochastic search. *ArXiv*, 2023.
- [7] J. Talairach and P. Tournoux. *Co-planar Stereotaxic Atlas of the Human Brain: 3-dimensional Proportional System : an Approach to Cerebral Imaging*. Thieme Publishers Series. G. Thieme, 1988.
- [8] John Mazziotta, Arthur Toga, Alan Evans, Peter Fox, Jack Lancaster, Karl Zilles, Roger Woods, Tomas Paus, Gregory Simpson, Bruce Pike, et al. A probabilistic atlas and reference system for the human brain: International consortium for brain mapping (icbm). *Philosophical Transactions of the Royal Society of London. Series B: Biological Sciences*, 356(1412):1293–1322, 2001.
- [9] David C Van Essen, Stephen M Smith, Deanna M Barch, Timothy EJ Behrens, Essa Yacoub, Kamil Ugurbil, Wu-Minn HCP Consortium, et al. The wu-minn human connectome project: an overview. *Neuroimage*, 80:62–79, 2013.
- [10] Michael J Arcaro, Mark A Pinsk, and Sabine Kastner. The anatomical and functional organization of the human visual pulvinar. *Journal of Neuroscience*, 35(27):9848–9871, 2015.
- [11] Emily J Allen, Ghislain St-Yves, Yihan Wu, Jesse L Breedlove, Jacob S Prince, Logan T Dowdle, Matthias Nau, Brad Caron, Franco Pestilli, Ian Charest, et al. A massive 7t fmri dataset to bridge cognitive neuroscience and artificial intelligence. *Nature neuroscience*, 25(1):116–126, 2022.
- [12] Christian F Beckmann, Marilena DeLuca, Joseph T Devlin, and Stephen M Smith. Investigations into resting-state connectivity using independent component analysis. *Philosophical Transactions of the Royal Society B: Biological Sciences*, 360(1457):1001–1013, 2005.
- [13] BT Thomas Yeo, Fenna M Krienen, Jorge Sepulcre, Mert R Sabuncu, Danial Lashkari, Marisa Hollinshead, Joshua L Roffman, Jordan W Smoller, Lilla Zöllei, Jonathan R Polimeni, et al. The organization of the human cerebral cortex estimated by intrinsic functional connectivity. *Journal of neurophysiology*, 2011.
- [14] Robert Tibshirani. Regression shrinkage and selection via the lasso. *Journal of the Royal Statistical Society Series B: Statistical Methodology*, 58(1):267–288, 1996.
- [15] Sungnyun Kim, Gihun Lee, Sangmin Bae, and Se-Young Yun. Mixco: Mix-up contrastive learning for visual representation. *arXiv preprint arXiv:2010.06300*, 2020.
- [16] Zixuan Liu, Ziqiao Wang, Hongyu Guo, and Yongyi Mao. Over-training with mixup may hurt generalization. *arXiv preprint arXiv:2303.01475*, 2023.
- [17] Aditya Ramesh, Prafulla Dhariwal, Alex Nichol, Casey Chu, and Mark Chen. Hierarchical text-conditional image generation with clip latents, 2022.
- [18] Kalanit Grill-Spector and Rafael Malach. The human visual cortex. *Annu. Rev. Neurosci.*, 27(1):649–677, 2004.

- [19] Yihui He, Xiangyu Zhang, and Jian Sun. Channel pruning for accelerating very deep neural networks. In *Proceedings of the IEEE international conference on computer vision*, pages 1389–1397, 2017.
- [20] Wei Wen, Chunpeng Wu, Yandan Wang, Yiran Chen, and Hai Li. Learning structured sparsity in deep neural networks. *Advances in neural information processing systems*, 29, 2016.
- [21] Alex Renda, Jonathan Frankle, and Michael Carbin. Comparing rewinding and fine-tuning in neural network pruning. *arXiv preprint arXiv:2003.02389*, 2020.
- [22] Tsung-Yi Lin, Michael Maire, Serge Belongie, James Hays, Pietro Perona, Deva Ramanan, Piotr Dollár, and C Lawrence Zitnick. Microsoft coco: Common objects in context. In *Computer Vision—ECCV 2014: 13th European Conference, Zurich, Switzerland, September 6–12, 2014, Proceedings, Part V 13*, pages 740–755. Springer, 2014.
- [23] Zhou Wang, Alan C Bovik, Hamid R Sheikh, and Eero P Simoncelli. Image quality assessment: from error visibility to structural similarity. *IEEE transactions on image processing*, 13(4):600–612, 2004.
- [24] Mathilde Caron, Ishan Misra, Julien Mairal, Priya Goyal, Piotr Bojanowski, and Armand Joulin. Unsupervised learning of visual features by contrasting cluster assignments. *Advances in neural information processing systems*, 33:9912–9924, 2020.
- [25] Christian Szegedy, Vincent Vanhoucke, Sergey Ioffe, Jon Shlens, and Zbigniew Wojna. Rethinking the inception architecture for computer vision. In *Proceedings of the IEEE conference on computer vision and pattern recognition*, pages 2818–2826, 2016.